Research

Characterization and photodegradation of methylene blue dye using bio-synthesized cerium oxide nanoparticles with *Spirulina platensis* extract

Mohamed H. H. Ali[1] · Mohamad S. Abdelkarim[2] · Afify D. G. Al-Afify[1]

Abstract

Increasing concern about environmental pollution attracts researchers to develop eco-friendly, low-cost, and sustainable approaches for green biosynthesis of nanoparticles to overcome pollutants. This study focuses on the green synthesis of ceria NPs using *Spirulina platensis* extract as a stabilizing and reducing agent. Characterization measurements, such as optical properties, X-ray diffraction, SEM, TEM, and FT-IR spectroscopy, confirmed the successful synthesis of crystalline and stable ceria NPs with well-defined morphological features. The calculated bandgaps energy of pure ceria, green CeO_2@Sp 2:1, and CeO_2@Sp 1:1 were 3.3, 3.15, and 2.94 eV, respectively. The as-synthesized and green ceria NPs showed an excellent degradation efficacy of MB dye under UV irradiation. Furthermore, the green ceria NPs showed high photodegradation efficiency of MB dye (R% = 86.2 and 88.8%) than pure ceria (R% = 76.4%) at certain specific conditions (pH = 11, contact time = 90 min, catalyst dose = 0.3 g/L and MB dye initial concentration = 100 mg/L). The isothermal constants confirmed that the degradation of MB dye is well-fitted with the Freundlich isotherm model ($R^2 > 0.99$) better than the Langmuir model ($R^2 < 0.8$). The kinetics models revealed a rapid degradation rate of MB dye, which follows pseudo-second-order models with C_e values ranging from 83.33 to 89.29 mg/g, with $R^2 > 0.99$. These results indicated the potential applicability and promising avenue for developing advanced ceria NPs for wastewater treatment applications.

Article highlights

1. Using a novel and facile method to prepare green synthesis ceria NPs using *Spirulina platensis* extract as a promising photocatalyst.
2. Providing a pioneering approach to preparing green ceria NPs as cheap and eco-friendly photocatalysts for the degradation of MB.
3. Demonstrating the high efficiency of green ceria NPs to eliminate methylene blue (MB) dye using green ceria NPs under UV light exposure.

✉ Mohamed H. H. Ali, mhha_ali@yahoo.com; Mohamad S. Abdelkarim, msk_saad@yahoo.com; Afify D. G. Al-Afify, afifydardeir@yahoo.com | ¹Chemistry Lab., Freshwater and Lakes Division, National Institute of Oceanography and Fisheries (NIOF), Cairo, Egypt. ²Hydrobiology Lab., Freshwater and Lakes Division, National Institute of Oceanography and Fisheries (NIOF), Cairo, Egypt.

1 Introduction

The massive progress of different industrial activities, especially those that use dyes and colored materials, such as ceramics, textiles, cosmetics, painting, and leathers, exacerbates the unbridled release of their effluents directly into the surrounding water surfaces. It poses an escalating and grave threat to the environment [1, 2]. The continuous discharge of untreated effluents results in water resources contamination and ecosystem deterioration, posing a significant threat to aquatic life, disrupting natural habitats, and endangering the health of humans and wildlife [3–5]. Addressing this serious issue demands new technologies for eliminating different pollutants and treating and regulating the industrial effluents discharged into the aquatic environment [6, 7].

Scientists exert great efforts to overcome this issue and develop several techniques for treating, eliminating, and degrading different pollutants from wastewater through biological, adsorption, and photodegradation techniques [8–13]. Conventional approaches, including physical and chemical preparations for dye degradation, encounter notable limitations and disadvantages. These include producing undesired-size NPs, which may require extensive time, elevated temperatures or pressures, or the potential formation of hazardous by-products. These circumstances may hinder their efficacy in addressing environmental concerns associated with textile dye pollution, making them economically and environmentally unsustainable [14, 15]. Green synthesis of nanoparticles involves utilizing natural resources, such as algae, microbes, and plant extracts, to synthesize novel nanoparticles [16]. The biosynthesis of nanoparticles significantly reduces the environmental impact, minimizing toxic substances and lowering energy usage [17, 18]. Furthermore, these technologies offer large-scale production, cost-effectiveness, eco-friendliness, and reduced energy consumption, making them more accessible for diverse applications, including catalysis, medicine, and environmental remediation [19–21]. The biogenic synthesis of nanoparticles promotes sustainable manufacturing and sharing to provide safe, innovative, and biocompatible nanomaterials that offer a more sustainable future [22–24].

Cerium is a rare earth metal from the lanthanides group. It is more abundant in the Earth's crust than lead and nearly as copper abundant [25]. This crucial element finds significant applications in modern technologies and various industries. It has a wide range of uses, particularly in environmental remediation, pharmaceuticals, and the production of glasses and ceramics [26–28]. Cerium possesses unique properties, such as a high oxygen storage capacity and excellent reactivity. Thus, it is widely used in automobile catalytic converters to mitigate air pollution by reducing harmful emissions. Cerium is a precious and indispensable element globally due to its wide applications and abundance [29]. Researchers fabricated CeO_2 with other oxides, such as CeO_2/In_2O_3 [30], $CeO_2/ZnO.4CdO$ [31], and NiV_2O_6/CeO_2 NPs [32]. Ceria NPs (CeO_2) are widely used in several applications, such as optical processes [33], photocatalysts [5, 7, 34], and medical purposes [35, 36].

The blue-green algae *S. platensis* is a vital microorganism containing numerous bioactive compounds, rich nutrient content, and potential health benefits. Its protein, vitamins, and minerals make it an all-in-one nutrient source for many individuals [37]. Moreover, *Spirulina* has rapidly grown in various environmental conditions, contributing to its availability on a global scale. It is widely used as a potential algae-based system for wastewater treatment. Many researchers used their extract as a stabilizing and reducing agent in the eco-friendly biosynthesis of NPs [38–42].

Fabricating ceria NPS with the extract of *S. platensis* is a novel and promising technique to produce nanoparticles without harmful chemicals or intensive energy consumption. Additionally, it is considered a new approach to addressing the knowledge gap in the existing methodologies [43, 44]. Many literatures showed methylene blue degradation dye using different types of catalysts, such as biogenic ZnO [23], CuSnSe [45], TiO_2@rGO [46], Er_2O_3-coated silicon [47], TiO_2 [48], manganese dioxide modified silicon nanowires [49], $TiO_2/SnO_2/CeO_2$ [50], and CeO_2 [51].

The main objective of this study was to characterize the optical and morphological properties of the bio-synthesized CeO_2@Sp NPs, besides demonstrating the ability of *S. platensis* to enhance the photodegradation efficiencies of ceria NPs to eliminate MB dye from aqueous solution under ultraviolet irradiation.

2 Materials and methods

2.1 Chemicals

$Ce(NO_3)_3·6H_2O$ (cerium nitrate hexahydrate), sodium hydroxide (NaOH), ammonium hydroxide (NH_4OH), ethylene glycol ($C_2H_6O_2$), ethanol (C_2H_5OH), citric acid ($C_6H_8O_7$) and methylene blue ($C_{16}H_{18}ClN_3S$) were of analytical grade (Sigma). All reagents were prepared using deionized water (DW).

2.2 Culturing of algal biomass

S. platensis strain was cultured according to the methods described by Zarrouk [52] and Bischoff and Bold [53] under specific conditions (24 °C, at pH 9–10, in a 16/8 h light/dark cycle and 3000 lx). The culture was shaken twice daily. After 21 days, the algal cells were harvested by centrifugation at 6000 rpm (Sigma 3–16 KL) for 10 min at 4 °C. The algal cells were rinsed several times with DW and dried at room temperature for 7 days. The algal mass was ground to a fine powder using an electric mill and sieved throughout a 63 µm sieve. 5 and 10 g of fine-dried algal biomass in two flasks containing 100 mL of distilled water were sonicated for 30 min and heated for 60 min at 90 °C with continuous stirring. After cooling, the mixtures were filtered through Whatman filter paper (No. 1). The pure filtrate was kept at 2–4 °C for further use.

2.3 Synthesis of CeO₂/*S. platensis* NPs

The modified Pechini method [54] was used for the preparation of ceria NPs (CeO₂ NPs) (Fig. 1). Deionized water (40 mL) was used to dissolve 12.5 g of $Ce(NO_3)_3 \cdot 6H_2O$, then ethylene glycol-citric acid (4:1) was added. CeO₂@Sp NPs were prepared by adding the aqueous extract of 5 g and 10 g of *Spirulina* biomass to separate flasks containing cerium nitrate solution. The mixture was stirred vigorously at 90 °C, forming a white precipitate of cerium hydroxide. After 6 h of continuous stirring, the homogenized mixtures were exposed to air for 26 h at 25 °C. Subsequently, the mixtures were centrifuged at 8000 r/min for 10 min, and the precipitate was dried at 120 °C for 6 h. The yellow cerium oxide obtained underwent further calcination at 500-550 °C for about 4 h using a muffle furnace (model, Nabrotherm p 180, Germany).

2.4 Physical characterizations

A spectrophotometer (Mettler Toledo V 670, United States) was used for UV-absorption spectroscopy examination at 200–800 nm. Band gap energy of as-prepared photocatalysts was calculated using UV-absorption spectra based on Tauc's equation [Eq. (1)]:

$$(\alpha h\upsilon)^2 = A\left(h\upsilon - E_g\right)$$
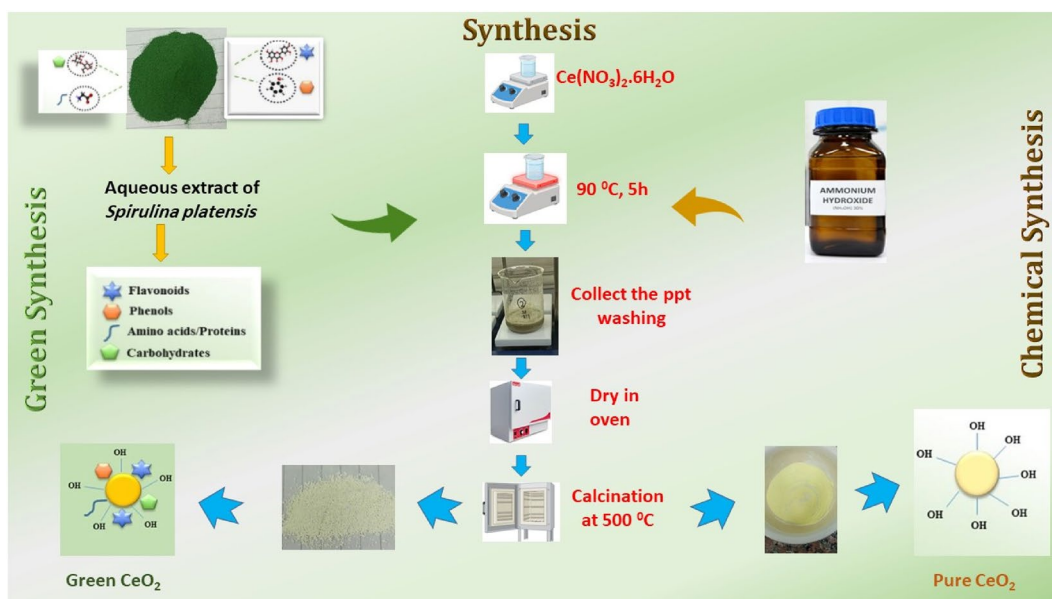
(1)

Fig. 1 Graphical schematic diagram illustrates the green and chemical preparation of CeO₂ NPs

An X-ray diffractometer (Philips, PW-3710) was used to determine the crystallographic structure of the as-prepared catalyst. The patterns of XRD were recorded by Cu-Kα radiation ($\lambda = 1.5408$ Å) at a tube voltage of 40 kV and current of 30 mA within a scan range of 20–80° at a scan rate of $2\theta = 5°$/min.

Scanning electron microscope (model, JEOL, JEM-2100, Japan) at an acceleration voltage of 200 kW was used to demonstrate the morphological characteristics (SEM and TEM) and determine the elemental composition (EDX) of as-prepared ceria NPs. Different functional groups in the surface area of as-prepared ceria NPs were detected using FTIR spectroscopy (model, 6700 FTIR, Nicolet, America) at 400–4000 cm^{-1} range.

2.5 Photocatalytic efficiency

The photocatalytic efficiency of the as-prepared catalyst was examined by photodegradation of MB using the batch method. The stock solution of MB (1 g/L) was used to prepare a standard 100 mg/L solution. The photodegradation reactions were carried out under UV irradiation (6 mercury lamps, 11 watts of each with light intensity of 50 lx at 260 nm). Before beginning photocatalytic experiments, all mixtures were stirred in the dark for 30 min to achieve the absorption–desorption equilibrium. The Main factors affecting MB dye's photodegradation (solutions' pH, catalyst dose, time of irradiation, and MB initial concentrations) were studied to obtain the optimum adsorption conditions for maximum degradation reactions. The concentrations of the remaining MB dye were evaluated at wavelength $\lambda = 665$ nm using a Jenway 6800 UV/VIS spectrophotometer. The photocatalytic process's capacity (q_e mg/g) and removal efficiency (R%) were calculated according to Eqs. (2) and (3).

$$q_e = \frac{(C_0 - C_e) \times V}{M} \tag{2}$$

$$R\% = \frac{(C_0 - C_e)}{C_0} \times 100 \tag{3}$$

where qe photocatalytic capacity (mg/g), R removal efficiency (%), V is the volume of MB dye (L); C_0 is the initial MB concentration; C_e is the equilibrium concentration of MB, and M is the mass of used catalyst (g).

2.6 Isotherms studies

Studying isotherm models provides valuable degradation process data, helping the researchers design and optimize efficient and sustainable solutions for various applications, especially environmental remediation and degradation of inorganic and organic pollutants. Langmuir, Freundlich, Dubinin, and Radushkevich's isotherm models designate the equilibrium results of the photocatalytic reactions. Langmuir model is expressed by the Eqs. (4) and (5).

$$\frac{1}{q_e} = \frac{1}{q_{max}} + \frac{1}{bq_{max}} \cdot \frac{1}{c_e} \tag{4}$$

Langmuir dimensionless constant (R_L) was evaluated from the following equation.

$$R_L = \frac{1}{1 + bC_e} \tag{5}$$

where q_{max} (mg/g) the maximum uptake of MB dye; q_e is the MB dye equilibrium concentration (mg/g); C_e mgL^{-1} the initial concentration of MB; and b (L/mg) constant of Langmuir.

Freundlich isotherm model is expressed as Eq. (6).

$$q_e = K_f C_e^{1/n} \tag{6}$$

where q_e (mg/g) is the amount of adsorbed MB dye; C_e (g/L) MB concentration at equilibrium; K_f is the adsorbent capacity, and n is the adsorption intensity.

Dubinin and Radushkevich represented by the Eqs. (7) and (8)

$$\ln q_e = \ln q_m - \beta\varepsilon^2 \tag{7}$$

$$E = \frac{1}{\sqrt{2\beta}} \tag{8}$$

where q_e is MB concentration at equilibrium (mg/g), q_m is maximum concentration of MB (mg/g), β is D-R isotherm constant (mol^2 kJ^{-2}), ε is the Polanyi potential (kJ/mol) and E mean free energy.

2.7 Kinetics studies

Studying kinetics models such as pseudo-first and pseudo-second-order reactions is essential in degradation and adsorption research. The kinetic models give much valuable data to illustrate the mechanisms of reactions between adsorbates and adsorbents, guiding the researchers to optimize reaction conditions to obtain effective adsorption processes for catalytic reactions.

Pseudo-first order and pseudo-second order models were studied according to the Eqs. (9) and (10).

$$\log\left(C_e - C_t\right) = \log C_e - \frac{k_1}{0.203}t \tag{9}$$

$$\frac{t}{C_t} = \frac{1}{k_2 C_e^2} + \frac{1}{C_e}t \tag{10}$$

where Ce and Ct are the concentration of MB dye (mg/g) at equilibrium and time "t" respectively; k1 (min^{-1}) and k2 (mg/g. min) are constant rate of pseudo-first order and pseudo-second-order reactions, respectively.

# 3 Results and discussion

3.1 UV-spectroscopy of ceria NPs

The study of UV–VIS spectroscopy of as-synthesized ceria and green ceria NPs gives valuable information of the electronic properties and NPs behavior according to their surface resonance, quantum confinement effects, and size-dependent bandgap shifts [14]. Figure 2a–c illustrates the UV–VIS spectrum for pure and as-synthesized green ceria NPs. The maximum absorption peak for pure CeO$_2$ was detected at 316 nm (Fig. 2a). A slight shift towards high wavelength (320 and 322 nm) was observed in the different doped ratios of the algal extract with ceria NPs (Fig. 2b and c). These shifts are according to modifications in the surface resonance and electronic band structure of green ceria NPS [55].

The band gap energy (Eg) was calculated using Tauc's equation [Eq. (1)]. A plot of (ahv)^2 versus hv was constructed to calculate Eg for the as-synthesized NPs (Fig. 2a–c). The calculated Eg values from this curve were 3.3, 3.15, and 2.94 eV for pure CeO$_2$, CeO$_2$@Sp 2:1, and CeO$_2$@Sp 1:1 NPs, respectively. A slight decrease of Eg values for green ceria NPs than pure ceria was detected. This decrease in Eg revealed that the algal extract improved the conductance and optical characteristics of CeO$_2$, enhancing their photocatalytic activities [50].

3.2 XRD spectra of CeO$_2$ NPs

XRD patterns of as-prepared catalysts of ceria and green ceria NPs are given in Fig. 3. The XRD diffractograms show four major peaks with high intensity are found at 2θ equal 28.44$^°$, 32.92$^°$, 47.32$^°$, and 56.14$^°$. These peaks were assigned to (111), (200), (220), and (311) planes according to standard JCPDS NO 89-8436. These principal planes typically confirmed the formation of the fluorite crystal structure of CeO$_2$. Hence, these peaks display well-defined and sharp peaks, revealing high purity and crystallinity formation of ceria NPs [14, 55]. The four minor peaks obtained at 2θ equal 58.18$^°$, 69.12$^°$, 76.85$^°$, and 78.78° were assigned to (222), (400), (331), and (420) planes. The slight broadening of detected peaks of the as-prepared green ceria NPs confirmed the successful formation of the bio-organic crystallization phase [56].

Fig. 2 UV–visible spectra and the band gaps energy of **a** pure CeO_2, **b** CeO_2@Sp 2:1 and **c** CeO_2@Sp 1:1 NPs
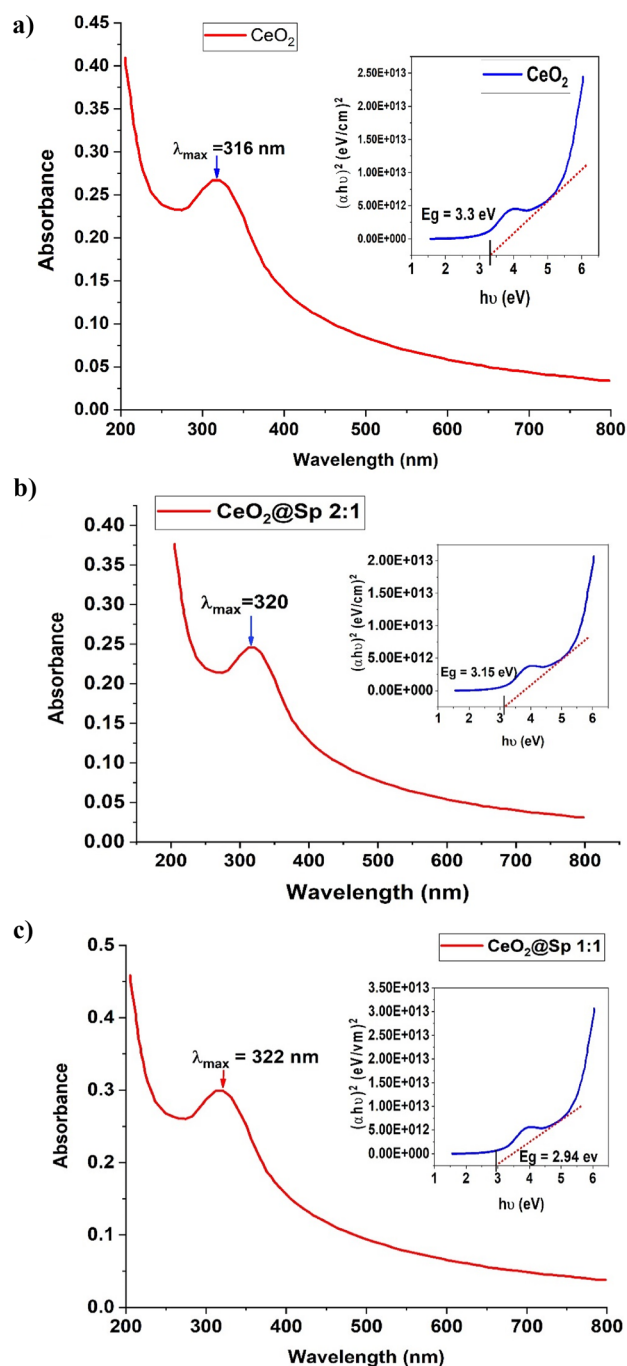
3.3 FTIR spectroscopy

FTIR spectroscopy describes the chemical composition and determines the surficial functional groups of NPs. The pure and green ceria NPs' FTIR spectra show several peaks corresponding to various molecular vibrations (Fig. 4). Pure CeO_2 showed several peaks at 3934 cm^{-1} attributed to O–H vibration [57], 3424 cm^{-1} assigned to the asymmetric stretching NH_2 band [58], 2923 and 2372 cm^{-1} belonging to C-H stretching and C=O stretching bonds, 1637 cm^{-1} assigned to the stretching C=C vibration bond and at 1091 cm^{-1} corresponding to =C–H group [34]. The broad peaks observed at 601 and 422 cm^{-1} revealed the formation of Ce–O bonds [59].

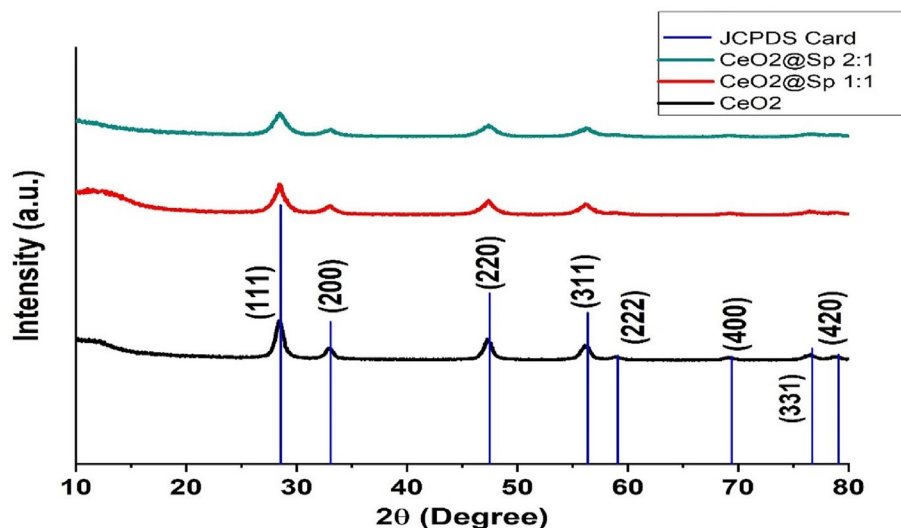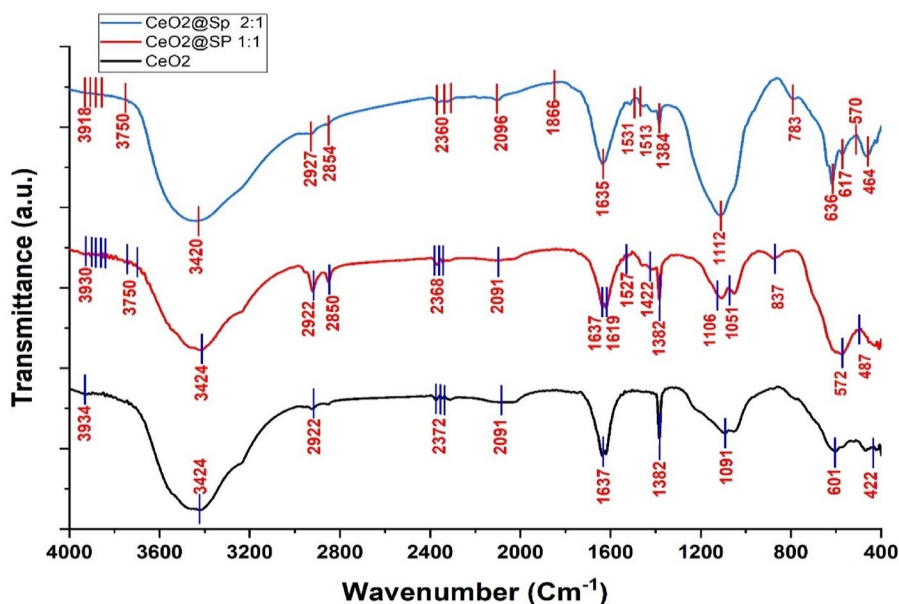**Fig. 3** XRD diffractogram of as synthesized ceria and green ceria NPs

Fig. 4 FTIR spectra of pure ceria and green synthesized CeO_2 with *spirulina* algal extract with different doping ratios

The impregnation of algal extracts at various doping ratios during the synthesis of ceria nanoparticles has notably influenced the functional groups. This often results in increased functional groups on the surface of the synthesized nanoparticles, as these extracts are abundant in bioactive compounds like polyphenols, polysaccharides, and proteins [60, 61]. The green ceria NPs showed several broad peaks at the 3930–3750 cm^{-1} range, assigned to the O–H vibration of alcoholic and water molecules [62]. Several peaks were observed between 2900 and 2000 cm^{-1} with particular wave numbers of 2921, 2850, 2343, and 2092 cm^{-1} attributed to carboxylic algal extract groups. Furthermore, strong peaks were found at 1635, 1619, 1531, and 1513 cm^{-1} assigned for C=C, carbonyl stretching C=O bond, and N–O bond [55].
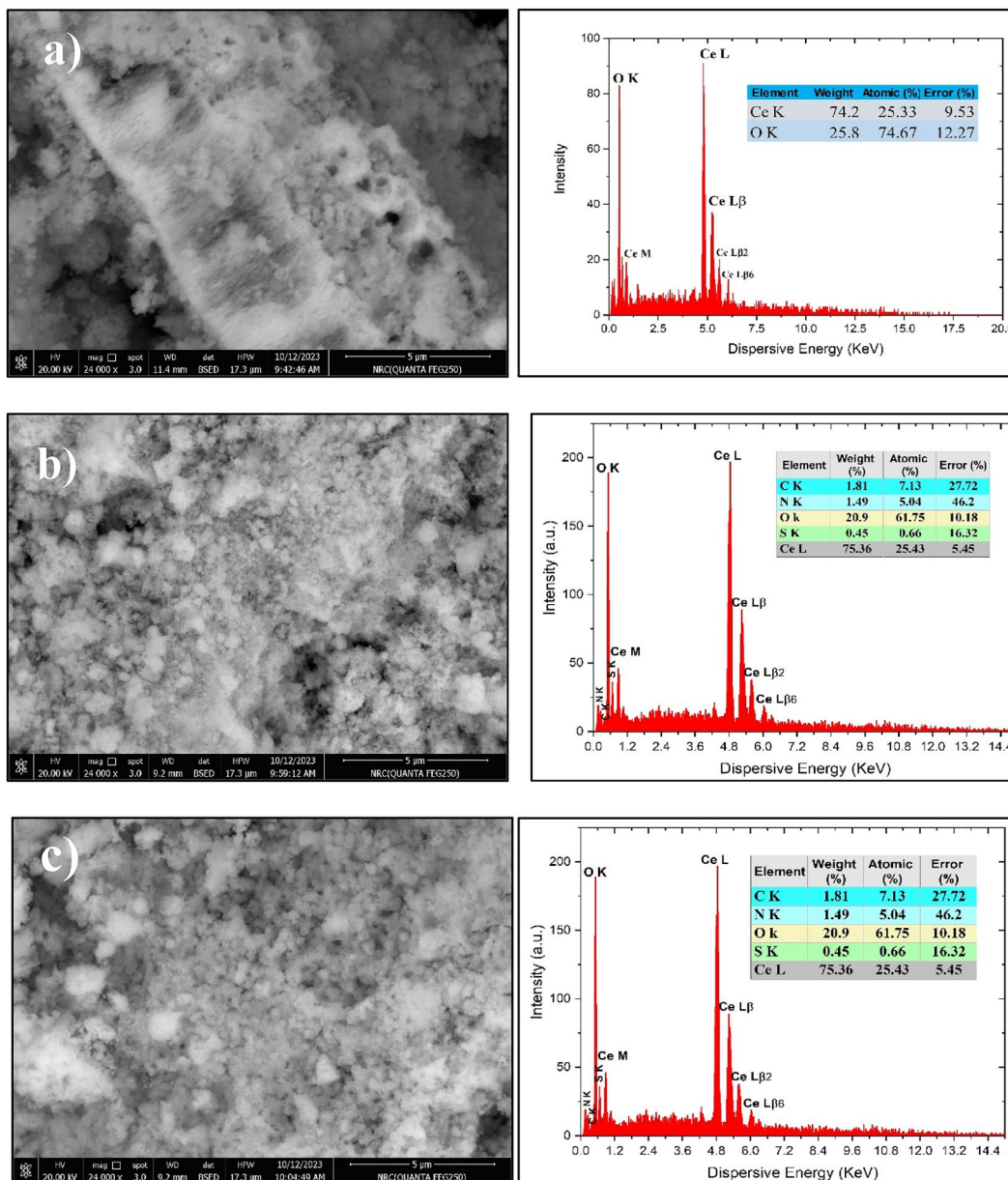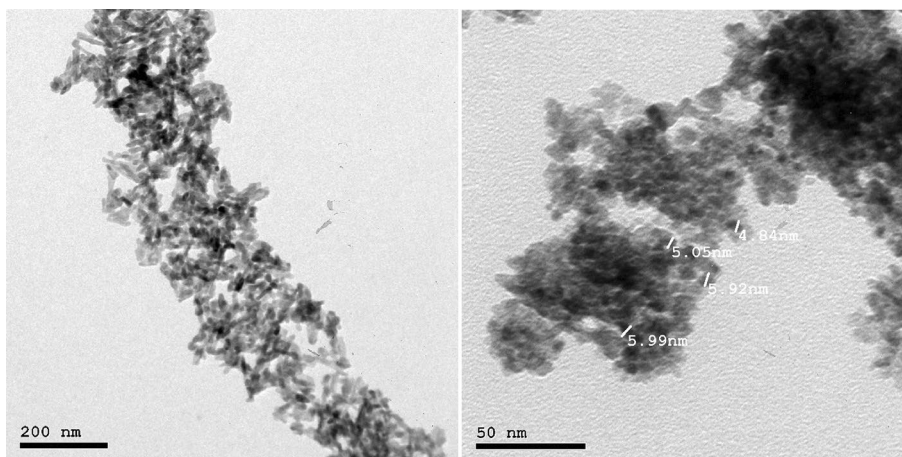
Fig. 5 SEM and EDX images of **a** pure CeO_2, **b** CeO_2@Sp 2:1 and **c** CeO_2@Sp 1:1

Fig. 6 TEM images of as-synthesized ceria NPs with different magnification power

3.4 SEM, EDX and TEM analyses of ceria and green ceria NPs

SEM images provide significant evidence about the morphological structure of ceria and green ceria NPs. SEM images (Fig. 5) exhibit spherical particles with irregular porous aggregation of CeO_2 clusters. The presence of porosity with irregular particle aggregation is owed to releasing gases during the calcination of catalysts [63].

EDX analysis is an excellent tool to determine the elemental structure of ceria NPs. Pure CeO2 nanoparticles exhibit two prominent peaks (Fig. 5), with cerium constituting 74.2% and oxygen 25.8%. Minor peaks, observed in Fig. 5a, appear to have negligible impact on the purity of the synthesized nanoparticles, confirming the formation of highly pure ceria. Green ceria nanoparticles displayed three additional minor peaks corresponding to C (3.06%), N (1.24%), and S (0.04%). These findings confirm the successful incorporation of pure CeO2 with organic compounds from the green extract of algal cells [64].

TEM images provide a high-resolution view of the morphology and structure of as-synthesized green and pure ceria NPs. The TEM images of ceria NPs appear as well-defined and often spherical particles with high contrast and uniform shape (Fig. 6).

The observed ceria particles agglomerate closely, forming a chain-like structure.

3.5 Photodegradation experiments

3.5.1 Effect of pH

pH significantly affects both the rate and the efficiency of the photodegradation reactions through its impacts on the ionization state of the adsorbate surface. Therefore, the degradation process exhibits optimal activities within specific pH ranges, indicating a pH-dependent nature of the degradation process [4].

The effect of pH on the photocatalytic degradation of MB dye was investigated in the range of 5–12 using an initial concentration of MB of 100 mg/L mixed with 0.3 g/L of as-synthesized ceria catalysts. A remarkable increase in MB dye decomposition with pH level elevation was observed (Fig. 7) under UV light for 90 min. The maximum removal percent was achieved at pH = 11 for all ceria NPs, with the highest removal efficiency of 79.28, 87.74, and 89% for pare CeO_2, CeO_2@Sp. (2:1) and CeO_2@Sp (1:1) NPs, respectively. The green synthesis of ceria particles with the algal extract of *S. platensis* improved and enhanced the degradation ability of the catalyst. However, the removal efficiency increased from 79.28% in the case of pare CeO_2 to 89% using CeO_2@Sp (2:1) NPs. At high pH levels, an excess of hydroxyl groups (OH) is released, generating free radicals (·OH) and accumulating negative charges on the surface of ceria nanoparticles. This accumulation creates strong electrostatic forces between the catalyst's surface and the cationic dye MB, facilitating the adsorption of dye particles. Consequently, an initiation of the degradation of dye particles occurred [65]. Pouretedal and Kadkhodaie [51], Ali et al. [46], and Kalaycıoğlu et al. [65] reported that optimum pH levels for maximum degradation of methylene blue are 11, 9, and 12, respectively (Table 1).

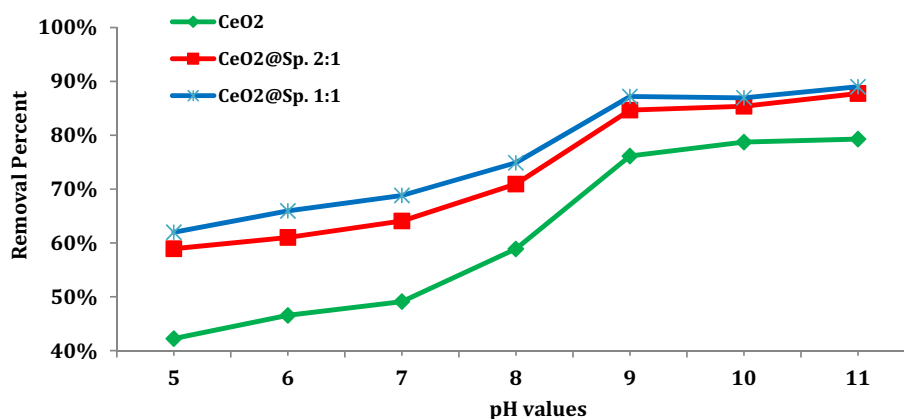**Fig. 7** Effect of pH level on the degradation process of MB dye

Table 1 Comparison of photodegradation efficiencies of some dyes using different photocatalysts

Organic substrate	Catalyst	pH	Dose (g/L)	Time (min)	Conc. (mg/L)	Eff. %	Ref
Congo red	CeO_2	7	0.3	120	50	98	[14]
Methylene blue	TiO_2@rGO	9	0.5	90	100	96	[46]
Methylene blue	CeO_2	11	1.0	125	5	98	[51]
Methylene blue	CeO_2	*	0.6	90	20	91	[55]
Methylene blue	CeO_2-NPs/GO	12	0.25	90	5	90	[65]
Methyl orange	ZnO	6.0	0.3	50	*	90	[67]
Methylene blue	CeO_2 coated on FACs (fly ash cenospheres)	*	4.0	300	10	60.0	[68]
Methylene blue	CeO_2	*	*	120	10	80	[70]
Methylene blue	CdS/SnO_2 NPs	*	0.1	180	50	90	[71]
Methylene blue	CeO_2	3	*	175	10	90	[72]
Rhodamine-B	TiO_2@rGO	9	0.2	60	30	99	[73]
Methylene blue	CeO_2 and CeO_2@Sp	11	0.3	90	100	89	This study

*: not available

Fig. 8 Effect of contact time on the photodegradation of MB dye
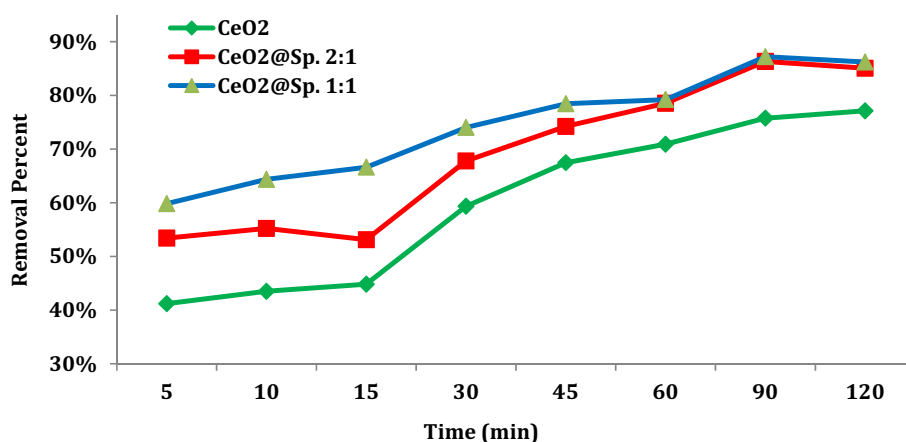
3.5.2 Effect of time

Contact time is a critical issue in understanding the kinetics of the photodegradation reactions, which directly affect the extent to which a substance degrades. The contact time effect on MB dye photodegradation (100 mg/L) was investigated at times ranging between 5 and 120 min with fixed solutions' pH = 9 (Fig. 8). A rapid degradation rate of MB was notable at the early reaction time of 5–45 min. The elevated degradation rate of MB is owed to the rapid formation of OH radicals, leading to a high adsorption affinity of as-synthesized catalysts. Over time, the reaction rate slows down due to the coverage of the photocatalyst's active sites with MB particles. Thus, the interaction between the photocatalyst surface and released photons ceased, leading to the cessation of the production of hydroxyl radicals [66].

The highest removal percentages of MB dye (75.5, 86.3, and 87.2%) were reached after 90 min (Fig. 8). Relative removal efficiency was achieved using green ceria NPs comparable to pare CeO_2 NPs. At the same time, there is no significant variation in degradation efficiency between different doped green ceria NPs with algal extract. These findings agree with Kusuma et al. [55], Ali et al. [46], and Kalaycıoğlu et al. [65], who mentioned the highest decomposition of MB at a contact time of 90 min using CeO_2, TiO_2@rGO, and CeO_2-NPs/GO NPs, respectively (Table 1).

3.5.3 Effect of dose

The photocatalyst dosage introduced is essential in eliminating different pollutants and remediating the hazards of organic particles during wastewater treatment. The effect of the different photocatalyst masses (0.05–0.5 g/L) on

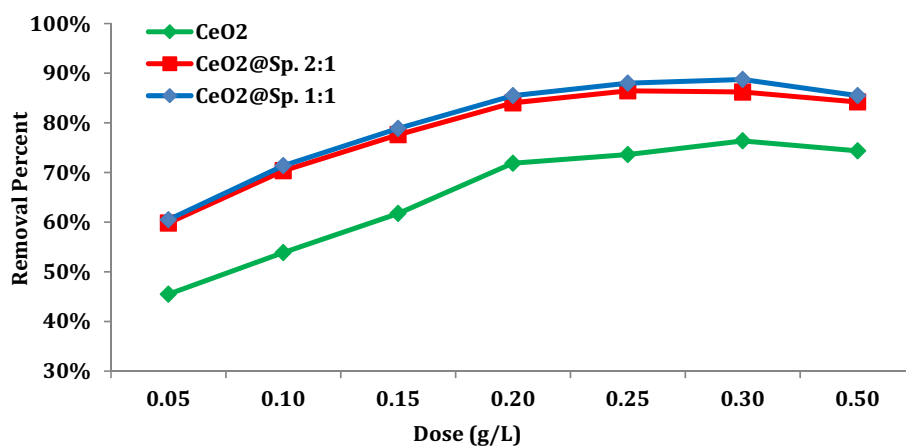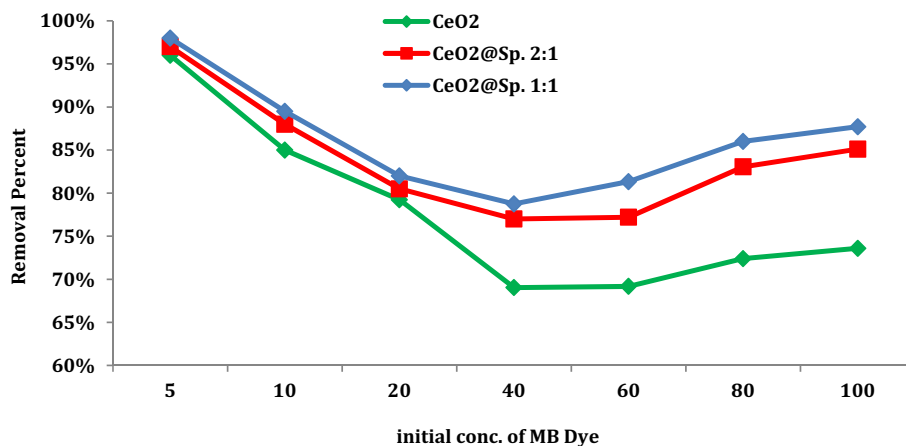**Fig. 9** Effect of photocatalyst dose on the photodegradation of MB dye

Fig. 10 Effect of initial concentration of MB dye on the photodegradation efficiency

the MB dye degradation process was examined at optimum specific conditions (Fig. 9). Increasing the photocatalyst dose enhanced the catalysts' active sites, leading to an easier, faster, and more effective MB decomposition rate. MB degradation rate showed a gradual increase with the increase of ceria and green ceria NPs, reaching maximum degradation removal efficiencies of 76.4, 86.2, and 88.8% at 0.3 g/L for pare CeO_2, CeO_2@Sp 2:1, and CeO_2@Sp 1:1 NPs, respectively. A further increase in photocatalyst dose leads to a decreased photodegradation process because of the aggregation of catalyst particles, so the solution becomes more turbid and prevents light penetration [50].

Zafar et al. [67] and Al-Onazi and Ali [14] postulated 0.3 g/L as the optimum catalyst dose for maximum degradation of MB using ZnO and CeO_2 NPs, respectively. While Zhang et al. [68] and Pouretedal and Kadkhodaie [51] reported 4.0 g/L and 1 g/L for degradation of MB using CeO_2 coated on FACs (fly ash cenospheres) and CeO_2 catalyst (Table 1).

3.5.4 Effect of initial dye concentration

Different serial concentrations (5–100 mg/L) of MB dye at a fixed pH of 11 and catalyst dose of 0.3 g/L were examined to detect the optimum initial dye concentration (Fig. 10). A remarkable high removal efficiency of MB dye (98%) was observed at low dye concentrations due to fewer dye molecules and high available active sites on the catalyst surface [69]. The degradation rate gradually decreased from 98% at 5 mg/L to about 88% at 100 mg/L of MB dye. The higher the dye concentrations, the lower the light penetration into the solution and the more occupation of the photocatalyst's active sites, leading to more competition between MB molecules. Murugan et al. [70] and El-Katori et al. [71] cited 10 and 50 mg/L as the optimum concentration of MB dye using CeO_2 and CdS/SnO_2 NPs, respectively (Table 1).

Table 2 Langmuir, Freundlich and Dubinin–Radushkevich isotherm constants for MB breakdown using pure and green ceria NPs

Catalyst	Langmuir isotherm				Freundlich isotherm			Dubinin–Radushkevich		
	b (L mg^{-1})	q_{max} (mg/g)	R_L	R^2	K_f [mg/g (L/mg)]	n	R^2	q_{max} mg/g	E (kJ mol^{-1})	R^2
CeO$_2$	0.05	17.99	0.16	0.79	0.95	1.87	0.99	40.67	408.2	0.84
CeO$_2$@Sp 2:1	0.08	8.01	0.11	0.78	1.79	0.82	0.98	49.14	500.0	0.81
CeO$_2$@Sp 1:1	0.09	11.09	0.10	0.73	0.56	0.49	0.99	62.64	408.2	0.86

Fig. 11 Langmuir isotherm model for degradation of MB dye on the surface of CeO$_2$ and green CeO$_2$@Sp NPs
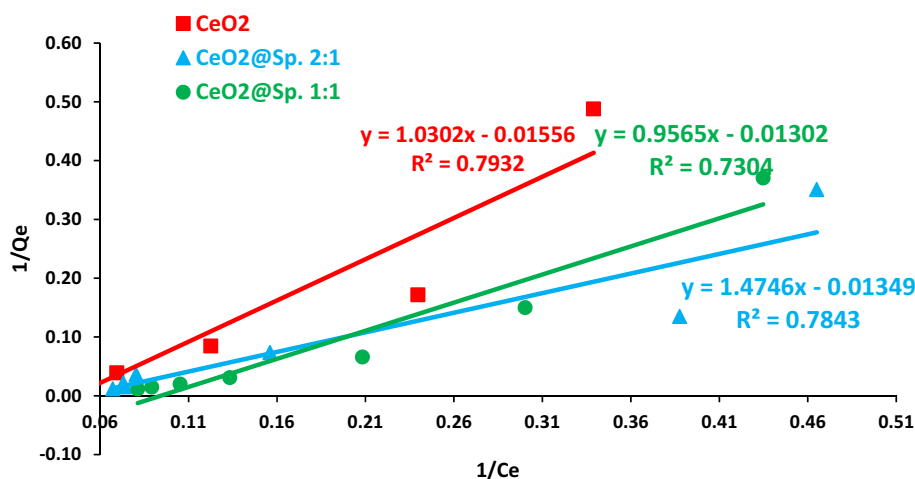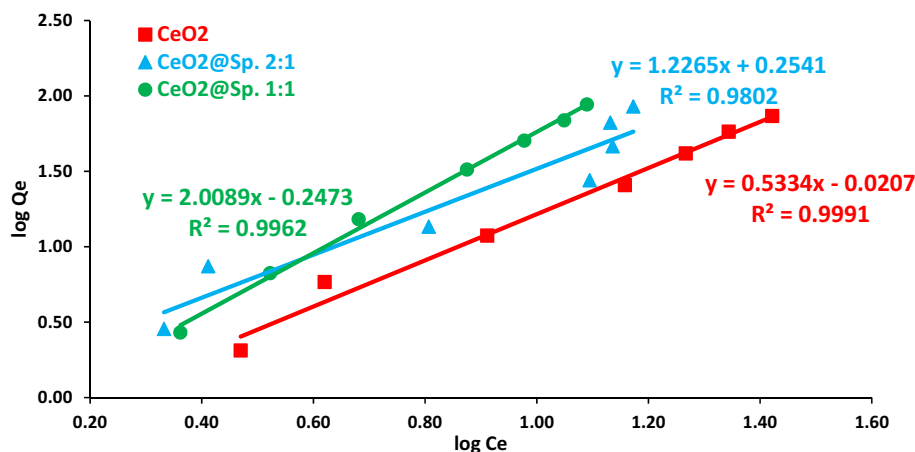

Fig. 12 Freundlich isotherm model for degradation of MB dye on the surface of CeO$_2$ and green CeO$_2$@Sp NPs

3.6 Isotherms studies

The studies of the isothermal models of organic pollutant degradation clearly illustrate the dye breakdown process at a constant temperature. Many isothermal models describe the relationship between the adsorption molecules onto the adsorbent surfaces. Langmuir isotherm model designates homogenous monolayer adsorption, while the Freundlich model pronounces multilayer adsorption. On the other hand, the Dubinin–Radushkevich isotherm considers the variation in the adsorption potential with surface coverage. Thus, it describes the adsorption in microporous and nanoporous materials.

Table 2 and Figs. 11, 12 and 13 present the calculated constants of studied isothermal models. The isothermal constants showed that the MB dye degradation using as-prepared ceria and green ceria NPs is well fitted with the FIM with $R^2 > 0.99$, better than LIM with $R^2 < 0.8$ (Table 1 and Figs. 11, 12 and 13). These results revealed that heterogeneous multilayer degradation of MB dye occurred. Ahsan et al. [1] and ElGarni et al. [2] found that the breakdown

Fig. 13 Dubinin Radushkevich isotherm model for the degradation of MB dye on the surface of CeO_2 and green CeO_2@Sp NPs
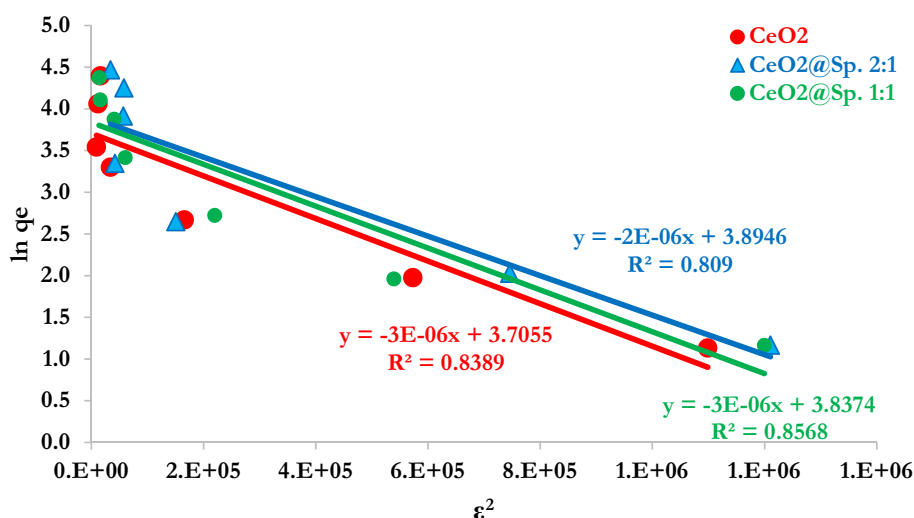

Table 3 Calculated constants of pseudo-first and pseudo-second order reactions for degradation of MB dye degradation on the surface of CeO_2 and green Ceo_2@Sp NPs

Catalyst	Pseudo-first order reaction			Pseudo-second order reaction		
	C_e (mg/g)	K_1 (min^{-1})	R^2	C_e (mg/g)	K_1 (min^{-1})	R^2
CeO_2	46.72	0.08	0.88	83.33	1.24E−03	0.99
CeO_2@Sp. 2:1	46.18	0.08	0.83	87.72	1.00E−03	0.99
CeO_2@Sp. 1:1	55.12	0.72	0.84	89.29	2.33E−0	0.99

Fig. 14 Pseudo-first order model for degradation of MB dye on the surface of CeO_2 and green CeO_2@Sp NPs
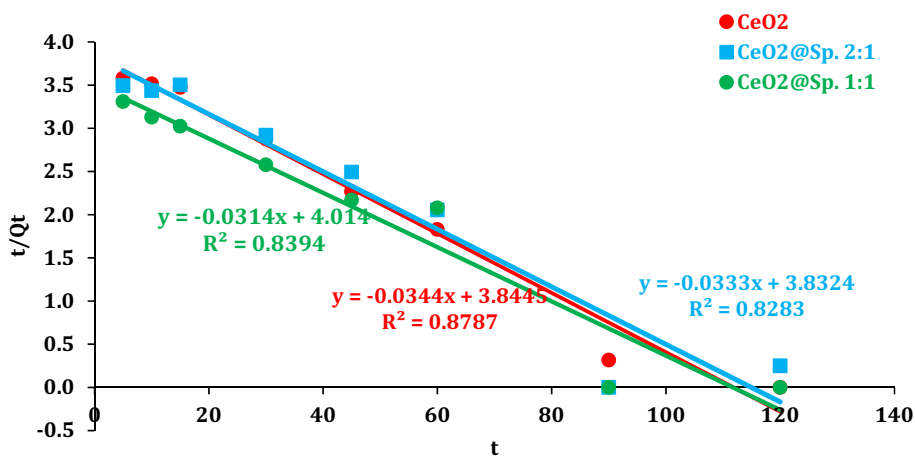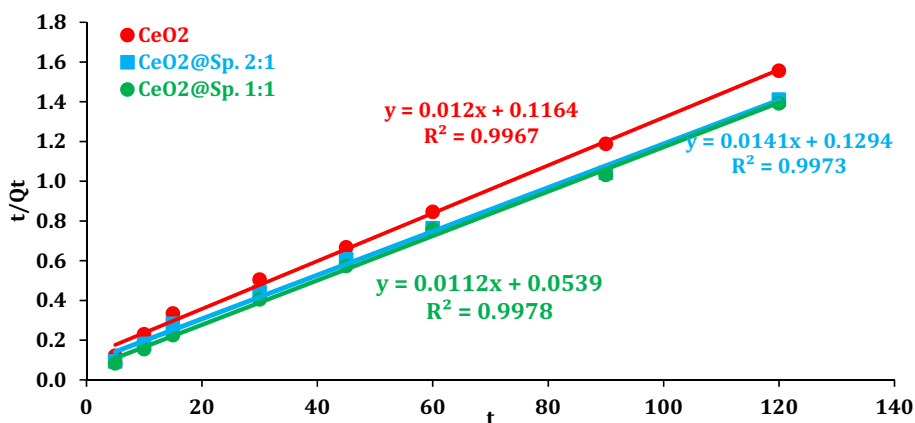

Fig. 15 Pseudo-second order model for degradation of MB dye on the surface of CeO_2 and green CeO_2@Sp NPs

of MB and 2,4 dinitrophenol using NiO/CuO-NC and green Fe_3O_4 NPs are a better fit with the Freundlich model than Langmuir isotherm model. The mean free energy (E kJ/mol) of the Dubinin–Radushkevich isotherm varied between 408.2 and 500.0 kJ/mol for the MB degradation. These values revealed that a chemisorption reaction occurred [74].

3.7 Kinetics models

Studying kinetics models of the adsorption provides essential information about the rate of adsorption reactions, helping to understand the dynamic nature of the degradation process, optimize reaction conditions, and predict the behavior of adsorbents over time. The most used kinetics models are pseudo-first order and pseudo-second order models, especially in the remediation of the pollutants in their aqueous solutions. The pseudo-first-order model indicated a linear correlation between the rate of adsorption and the difference between adsorbate concentrations at initial and equilibrium status. The pseudo-second-order model gives a linear relation between the adsorption rate and the square of the difference between adsorbate concentrations at initial and equilibrium status.

The results of kinetic models (Table 3 and Figs. 14 and 15) showed that the degradation of MB dye followed the pseudo-second-order model with a C_e range of 83.33 and 89.29 mg/g with $R^2 > 0.99$.

4 Conclusion

The green synthesis of ceria (NPs) with *S. platensis* extracts provides an environmentally promising approach to sustainable development. Utilizing natural extracts, especially from algae, introduces bioactive compounds that enhance the resulting ceria NPs' properties and ensure the novel catalysts' eco-friendly fabrication. Physical characterization confirmed the high purity and polycrystalline formation of ceria NPs. Optical UV–VIS spectra indicated the formation of ceria NPs, evident from intense peaks at 316, 320, and 322 nm. These peaks indicated a decrease in bandgap energy with an increase in the doping ratio of the algal extract. FTIR measurements showed multi-functional groups due to impregnating pure ceria with the algal extract. EDX results confirmed the introduction of C, N, and S elements from the algal extract to green ceria NPs with different abundance ratios. The green ceria NPs showed higher removal efficiency of MB dye (R% = 86.2 and 88.8%) than pure ceria (R% = 76.4%) under specific conditions (pH = 11, 90 min contact time, 0.3 g/L catalyst dose and 100 mg/L MB initial concentration). The isothermal constants showed that the MB dye degradation is well fitted with the Freundlich model with $R^{2} > 0.99$, better than the Langmuir model with $R^2 < 0.8$. Furthermore, the degradation of MB dye followed a pseudo-second-order model with C_e values ranging between 83.33 and 89.29 mg/g with $R^2 > 0.99$.

Data availability All data generated or analyzed during this study are included in this published article.

Code availability Non applicable.

Declarations

Ethics approval Not applicable.

Consent to participate All authors voluntarily agree to participate in this research study.

Consent for publication All authors voluntarily approved the publication of this research study.

Competing interests The authors have no competing interests to declare that are relevant to the content of this article.

References

1. Ahsan H, Shahid M, Imran M, Mahmood F, Siddique MH, Ali HM, et al. Photocatalysis and adsorption kinetics of azo dyes by nanoparticles of nickel oxide and copper oxide and their nanocomposite in an aqueous medium. PeerJ. 2022;10: e14358.

2. AlGarni TS, Ali MH, Al-Mohaimeed AM. Green biosynthesis of Fe_3O_4 nanoparticles using Chlorella vulgaris extract for enhancing degradation of 2, 4 dinitrophenol. J King Saud Univ Sci. 2023;35(1): 102426. https://doi.org/10.1016/j.jksus.2022.102426.

3. Al-Onazi WA, Ali MH, AlGarni T. Using pomegranate peel and date pit activated carbon for the removal of cadmium and lead ions from aqueous solution. J Chem. 2021. https://doi.org/10.1155/2021/5514118.

4. Ali MH, Goher ME, Al-Afify AD, El-Sayed SM. A facile method for synthesis rGO/Ag nanocomposite and its uses for enhancing photocatalytic degradation of Congo red dye. SN Appl Sci. 2022;4(10):276. https://doi.org/10.1007/s42452-022-05163-0.

5. Al-Enazi NM, Alwakeel S, Alhomaidi E. Photocatalytic and biological activities of green synthesized SnO2 nanoparticles using *Chlorella vulgaris*. J Appl Microbiol. 2022;133(6):3265–75. https://doi.org/10.1111/jam.15607.

6. Ali MH, Al-Qahtani KM, El-Sayed SM. Enhancing photodegradation of 2,4,6 trichlorophenol and organic pollutants in industrial effluents using nanocomposite of TiO_2 doped with reduced graphene oxide. Egypt J Aquat Res. 2019;45(4):321–8. https://doi.org/10.1016/j.ejar.2019.08.003.

7. Wu J, Li Q, Zhang G, Lv Y. Synthesis, characterization, and photocatalysis of a rare-earth cerium/silver/zinc oxide inorganic nanocomposite. Green Process Synth. 2022;11(1):503–11. https://doi.org/10.1515/gps-2022-0051.

8. Ali MH, Abd Elkarim MS, Haroun S, Attwa K. Bioremediation of Fe, Zn and Cd ions from aqueous solution using died cells of cyanobacterial mats from extreme habitat, Siwa Oasis, Egypt. Egypt J Aquat Biol Fish. 2019;22(5):511–22. https://doi.org/10.21608/EJABF.2019.25914.

9. Al-Qahtani KM, Ali MH, Al-Afify AG. Synthesis and use of TiO_2@ rGO nanocomposites in photocatalytic removal of chromium and lead ions from wastewater. J Elementol. 2020;25(1):315–22. https://doi.org/10.5601/jelem.2019.24.2.1862.

10. Shojaee A, Mostafavi A, Shamspur T, Fathirad F. Green synthesis of cerium oxide nanoparticles: Characterization, parameters optimization and investigation of photocatalytic application. Biointerface Res Appl Chem. 2020;10:5932–7. https://doi.org/10.33263/BRIAC104.932937.

11. Rozhin P, Melchionna M, Fornasiero P, Marchesan S. Nanostructured ceria: biomolecular templates and (bio) applications. Nanomaterials. 2021;11(9):2259. https://doi.org/10.3390/nano11092259.

12. Sabouri Z, Sabouri M, Amiri MS, Khatami M, Darroudi M. Plant-based synthesis of cerium oxide nanoparticles using Rheum turkestanicum extract and evaluation of their cytotoxicity and photocatalytic properties. Mater Technol. 2022;37(8):555–68. https://doi.org/10.1080/10667857.2020.1863573.

13. Al-Qahtani KM, Abd Elkarim MS, Al-Fawzan FF, Al-Afify AD, Ali MH. Biosorption of hexavalent chromium and molybdenum ions using extremophilic cyanobacterial mats: efficiency, isothermal, and kinetic studies. Int J Phytorem. 2023. https://doi.org/10.1080/15226514.2023.2232878.

14. Al-Onazi WA, Ali MH. Synthesis and characterization of cerium oxide hybrid with chitosan nanoparticles for enhancing the photodegradation of Congo Red dye. J Mater Sci Mater Electron. 2021;32:12017–30. https://doi.org/10.1007/s10854-021-05832-7.

15. Bhole R, Gonsalves D, Murugesan G, Narasimhan MK, Srinivasan NR, Dave N, et al. Superparamagnetic spherical magnetite nanoparticles: synthesis, characterization and catalytic potential. Appl Nanosci. 2023;13(9):6003–14.

16. Vinayagam R, Nagendran V, Goveas LC, Narasimhan MK, Varadavenkatesan T, Chandrasekar N, Selvaraj R. Structural characterization of marine macroalgae derived silver nanoparticles and their colorimetric sensing of hydrogen peroxide. Mater Chem Phys. 2024;313: 128787.

17. Zamani A, Marjani AP, Alimoradlu K. Walnut shell-templated ceria nanoparticles: green synthesis, characterization and catalytic application. Int J Nanosci. 2018;17:1850008. https://doi.org/10.1142/S0219581X18500084.

18. Ishak NA, Kamarudin SK, Timmiati SN. Green synthesis of metal and metal oxide nanoparticles via plant extracts: An overview. Mater Res Express. 2019;6: 112004. https://doi.org/10.3390/ijms242015397.

19. Govarthanan M, Liang Y, Kamala-Kannan S, Kim W. Ecofriendly and sustainable green nano-technologies for the mitigation of emerging environmental pollutants. Chemosphere. 2022;287: 132234.

20. Yao X, BahrAluloom YJ, Jawad SF, Abdtawfeeq TH, Al-janabi DR, Ahmad N, et al. Multipurpose properties the Z-scheme dimanganese copper oxide/cadmium sulfide nanocomposites for photo-or photoelectro-catalytic, antibacterial applications, and thiamine detection process. J Photochem Photobiol A Chem. 2023;436: 114374.

21. Chen Y, Jihad A, Hussam F, Al-Abdeen SHZ, Hussein JM, Adhab ZH, et al. A facile preparation method for efficiency a novel $LaNiO_3$/$SrCeO_3$ (pn type) heterojunction catalyst in photocatalytic activities, bactericidal assessment and dopamine detection. Surf Interfaces. 2023;38: 102830.

22. Dikshit PK, Kumar J, Das AK, Sadhu S, Sharma S, Singh S, et al. Green synthesis of metallic nanoparticles: applications and limitations. Catalysts. 2021;11(8):902. https://doi.org/10.3389/fbioe.2022.874742.

23. Abbas A, Ahmad T, Hussain S, Noman M, Shahzad T, Iftikhar A, Cheema A, Ijaz M, Tahir M, Gohari G, Li B, Mahmood F, Shahid M. Immobilized biogenic zinc oxide nanoparticles as photocatalysts for degradation of methylene blue dye and treatment of textile effluents. Int J Environ Sci Technol. 2022;19:11333–46. https://doi.org/10.1007/s13762-021-03872-4.

Discover

24. Sridevi H, Bhat MR, Kumar PS, Kumar NM, Selvaraj R. Structural characterization of cuboidal α-Fe₂O₃ nanoparticles synthesized by a facile approach. Appl Nanosci. 2023. https://doi.org/10.1007/s13204-023-02780-y.

25. Ma R, Zhang S, Wen T, Gu P, Li L, Zhao G, Niu F, Huang Q, Tang Z, Wang X. A critical review on visible-light-response CeO₂-based photo-catalysts with enhanced photooxidation of organic pollutants. Catal Today. 2019;335:20–30. https://doi.org/10.1016/j.cattod.2018.11.016.

26. Arumugam A, Karthikeyan C, Hameed ASH, Gopinath K, Gowri S, Karthika V. Synthesis of cerium oxide NPs using *Gloriosa superba* L. leaf extract and their structural, optical and antibacterial properties. Mater Sci Eng C. 2015;49:408–15. https://doi.org/10.1016/j.msec.2015.01.042.

27. Dai J, Guo Y, Xu L, Zhuang G, Zheng Y, Sun D, Huang J, Li Q. Bovine serum albumin templated porous CeO₂ to support Au catalyst for benzene oxidation. Mol Catal. 2020;486: 110849. https://doi.org/10.1016/j.mcat.2020.110849.

28. Zhao W, Wei Z, Zhang X, Ding M, Huang S, Yang S. Magnetic recyclable MnFe₂O₄/CeO₂/SnS₂ ternary nano-photocatalyst for photo-Fenton degradation. Appl Catal A: Gen. 2020;593: 117443. https://doi.org/10.1016/j.apcata.2020.117443.

29. Alqarni LS, Alghamdi MD, Alshahrani AA, Nassar AM. Green nanotechnology: recent research on bioresource-based nanoparticle synthesis and applications. J Chem. 2022. https://doi.org/10.1155/2022/4030999.

30. Ganie AS, Bashar N, Bano S, Hijazi S, Sultana S, Sabir S, Khan MZ. Development and application of redox active GO supported CeO₂/In₂O₃ nanocomposite for photocatalytic degradation of toxic dyes and electrochemical detection of sulfamaxole. Surf Interfaces. 2023;38: 102774.

31. Zhao B, Wang JS, Zheng J, Wu Y, Wang CC. Performance analysis of humidity sensor prepared by CeO₂/molecular sieves type 4A composite. Mater Lett. 2023;330: 133345.

32. Mahdi AA, Obeid RA, Abdullah K, Mohammed S, Kadhim AJ, Ramadan MF, et al. A facile construction of NiV₂O₆/CeO₂ nano-heterojunction for photo-operated process in water remediation reaction, antibacterial studies, and detection of D-Amino acid in peroxidase system. Surf Interfaces. 2023;40:102970.

33. Fu YP, Wen SB, Lu CH. Preparation and characterization of samaria-doped ceria electrolyte materials for solid oxide fuel cells. J Am Ceram Soc. 2008;91(1):127–31. https://doi.org/10.1111/j.1551-2916.2007.01923.x.

34. Khan MA, Siddique MAR, Sajid M, Karim S, Ali MU, Abid R, Bokhari SAI. A comparative study of green and chemical cerium oxide nanoparticles (CeO₂-NPs): from synthesis, characterization, and electrochemical analysis to multifaceted biomedical applications. BioNanoScience. 2023. https://doi.org/10.1007/s12668-023-01114-0.

35. Sangsefidi FS, Nejati M, Verdi J, Salavati-Niasari M. Green synthesis and characterization of cerium oxide nanostructures in the presence carbohydrate sugars as a capping agent and investigation of their cytotoxicity on the mesenchymal stem cell. J Clean Prod. 2017;156:741–9. https://doi.org/10.1016/j.jclepro.2017.04.114.

36. Rajeshkumar S, Naik P. Synthesis and biomedical applications of cerium oxide nanoparticles—a review. Biotechnol Rep. 2018;17:1–5. https://doi.org/10.1016/j.btre.2017.11.008.

37. Belay A, Ota Y, Miyakawa K, Shimamatsu H. Current knowledge on potential health benefits of *Spirulina*. J Appl Phycol. 1993;5:235–41.

38. Mahdieh M, Zolanvari A, Azimee AS. Green biosynthesis of silver nanoparticles by *Spirulina platensis*. Sci Iran. 2012;19(3):926–9. https://doi.org/10.1016/j.scient.2012.01.010.

39. Gunasundari E, Senthil Kumar P, Christopher FC, Arumugam T, Saravanan A. Green synthesis of metal nanoparticles loaded ultrasonic-assisted *Spirulina platensis* using algal extract and their antimicrobial activity. IET Nanobiotechnol. 2017;11(6):754–8.

40. Vasanth V. Synthesis of titanium dioxide nanoparticles using *Spirulina platensis* algae extract. Pharma Innov J 2022;266–9. https://doi.org/10.22271/tpi.2022.v11.i7Sd.13643.

41. Rashad SA, El-Chaghaby G, Elchaghaby AM. Antibacterial activity of silver nanoparticles biosynthesized using *Spirulina platensis* microalgae extract against oral pathogens. Egypt J Aquat Biol Fish. 2019;23(5):261–6.

42. El-Kheir A, Abd-Elqader SH, Helal AM, Farroh KH. Synthesis of silver nanoparticles using *Ulva lactuca, Sargassum denticulatum, Spirulina platensis* and *Chlorella vulgaris*. J Sci Res Sci. 2021;38:142–67 (**Part 2 (Biological Sciences)**).

43. Sidorowicz A, Margarita V, Fais G, Pantaleo A, Manca A, Concas A, Cao G. Characterization of nanomaterials synthesized from *Spirulina platensis* extract and their potential antifungal activity. PLoS ONE. 2022;17(9): e0274753. https://doi.org/10.1371/journal.pone.0274753.

44. Vasanth V, Murugesh KA, Susikaran S. Synthesis of titanium dioxide nanoparticles using *Spirulina platensis* algae extract. Pharma Innov J. 2022. https://doi.org/10.2227/tpi.2022.v11.i7Sd.13643.

45. Patel K, Parangi T, Solanki GK, Mishra MK, Patel KD, Pathak VM. Photocatalytic degradation of methylene blue and crystal violet dyes under UV light irradiation by sonochemically synthesized CuSnSe nanocrystals. Eur Phys J Plus. 2021;136:1–17. https://doi.org/10.1140/epjp/s13360-021-01725-0.

46. Ali MH, Goher ME, Al-Afify AD. Kinetics and adsorption isotherm studies of methylene blue photodegradation under UV irradiation using reduced graphene oxide-TiO₂ nanocomposite in different wastewaters effluents. Egypt J Aquat Biol Fish. 2019;23(1):253–63. https://doi.org/10.21608/ejabf.2019.26975.

47. Brik A, Naama S, Hadjersi T, Benamar MEA, Bouanik S, Manseri A. Photodegradation of methylene blue under UV and visible light irradiation by Er₂O₃-coated silicon nanowires as photocatalyst. React Kinet Mech Catal. 2020;131(1):525–36. https://doi.org/10.1007/s11144-020-01862-0.

48. Che Ramli ZA, Asim N, Isahak WN, Emdadi Z, Ahmad-Ludin N, Yarmo MA, Sopian K. Photocatalytic degradation of methylene blue under UV light irradiation on prepared carbonaceous. Sci World J. 2014. https://doi.org/10.1155/2014/415136.

49. Gao W, Shao M, Yang L, Zhuo S, Ye S, Lee S-T. Manganese dioxide modified silicon nanowires and their excellent catalysis in the decomposition of methylene blue. Appl Phys Lett. 2012;100: 063104. https://doi.org/10.1063/1.3682486.

50. Husna RA, Natsir TA. Enhancing photocatalytic degradation of methylene blue by mixed oxides TiO₂/SnO₂/CeO₂ under visible light. Res Eng. 2023;19: 101253. https://doi.org/10.1016/j.rineng.2023.101253.

51. Pouretedal HR, Kadkhodaie A. Synthetic CeO₂ nanoparticle catalysis of methylene blue photodegradation: kinetics and mechanism. Chin J Catal. 2010;31(11–12):1328–34. https://doi.org/10.1016/S1872-2067(10)60121-0.

52. Zarrouk C. Contribution à l'étude d'une cyanophycée. Influence de divers' facteurs physiques et chimiques sur la croissance et la photosynthèse de *Spirulina maxima*. (Setch et Gardner) Geitler. Ph.D. Thesis, Université de Paris, Paris, France; 1966.

53. Bischoff HW, Bold HC. Phycological studies IV. Some soil algae from enchanted rock and related algal species. Texas: University of Texas Publications; 1963. p. 1–95.

54. Calvache-Muñoz J, Prado FA, Rodriguez-Paez JE. Cerium oxide nanoparticles: synthesis, characterization and tentative mechanism of particle formation. Colloids Surf A Physicochem Eng Asp. 2017;529:146–59. https://doi.org/10.1016/j.colsurfa.2017.05.059.

55. Kusuma KB, Manju M, Ravikumar CR, Raghavendra N, Amulya MS, Nagaswarupa HP, Shekhar TS. Photocatalytic degradation of methylene blue and electrochemical sensing of paracetamol using cerium oxide nanoparticles synthesized via sonochemical route. Appl Surf Sci Adv. 2022;11: 100304. https://doi.org/10.1016/j.apsadv.2022.100304.

56. Kurajica S, Minga I, Guliš M, Mandić V, Simčić I. High surface area ceria nanoparticles via hydrothermal synthesis experiment design. J Nanomater. 2016. https://doi.org/10.1155/2016/7274949.

57. Surendra TV, Roopan SM. Photocatalytic and antibacterial properties of phytosynthesized CeO$_2$ NPs using *Moringa oleifera* peel extract. J Photochem Photobiol B Biol. 2016;161:122–8.

58. Jayakumar G, Irudayaraj AA, Raj AD. Investigation on the synthesis and photocatalytic activity of activated carbon–cerium oxide (AC–CeO$_2$) nanocomposite. Appl Phys A. 2019;125(11):1–9.

59. Senthilkumar RP, Bhuvaneshwari V, Ranjithkumar R, Sathiyavimal S, Malayaman V, Chandarshekar B. Synthesis, characterization and anti-bacterial activity of hybrid chitosan–cerium oxide nanoparticles: as a bionanomaterials. Int J Biol Macromol. 2017;104:1746–52. https://doi.org/10.1016/j.ijbiomac.2017.03.139.

60. Sharma JK, Srivastava P, Ameen S, Akhtar MS, Sengupta SK, Singh G. Phytoconstituents assisted green synthesis of cerium oxide nano-particles for thermal decomposition and dye remediation. Mater Res Bull. 2017;91:98–107. https://doi.org/10.1016/j.materresbull.2017.03.034.

61. Soror AFS, Ahmed MW, Hassan AE, Alharbi M, Alsubhi NH, Al-Quwaie DA, Abdalla H. Evaluation of green silver nanoparticles fabricated by *Spirulina platensis* phycocyanin as anticancer and antimicrobial agents. Life. 2022;12(10):1493. https://doi.org/10.3390/life12101493.

62. Masood N, Irshad MA, Nawaz R, Abbas T, Abdel-Maksoud MA, AlQahtani WH, Abeed AH. Green synthesis, characterization and adsorption of chromium and cadmium from wastewater using cerium oxide nanoparticles, reaction kinetics study. J Mol Struct. 2023;1294: 136563. https://doi.org/10.1016/j.molstruc.2023.136563.

63. Farahmandjou M, Zarinkamar M, Firoozabadi TP. Synthesis of cerium oxide (CeO$_2$) nanoparticles using simple Co-precipitation method. Rev Mex Fís. 2016;62(5):496–9.

64. Muthuvel A, Jothibas M, Mohana V, Manoharan C. Green synthesis of cerium oxide nanoparticles using *Calotropis procera* flower extract and their photocatalytic degradation and antibacterial activity. Inorg Chem Commun. 2020;119: 108086. https://doi.org/10.1016/j.inoche.2020.108086.

65. Kalaycıoğlu Z, Özuğur Uysal B, Pekcan O, Erim FB. Efficient photocatalytic degradation of methylene blue dye from aqueous solution with cerium oxide nanoparticles and graphene oxide-doped polyacrylamide. ACS Omega. 2023;8(14):13004–15. https://doi.org/10.1021/acsomega.3c00198.

66. Jaramillo-Fierro X, González S, Medina F. La-doped ZnTiO$_3$/TiO$_2$ nanocomposite supported on ecuadorian diatomaceous earth as a highly efficient photocatalyst driven by solar light. Molecules. 2021;26(20):6232. https://doi.org/10.3390/molecules26206232.

67. Zafar MN, Dar Q, Nawaz F, Zafar MN, Iqbal M, Nazar MF. Effective adsorptive removal of azo dyes over spherical ZnO nanoparticles. J Market Res. 2019;8(1):713–25.

68. Zhang J, Bing WA, Hao CU, Chuang LI, Jianping ZH, Qin LI. Synthesis of CeO$_2$/fly ash cenospheres composites as novel photocatalysts by modified pyrolysis process. J Rare Earths. 2014;32(12):1120–5. https://doi.org/10.1016/S1002-0721(14)60192-7.

69. Hassan MM, Carr CM. Biomass-derived porous carbonaceous materials and their composites as adsorbents for cationic and anionic dyes: a review. Chemosphere. 2021;265: 129087. https://doi.org/10.1016/j.chemosphere.2020.129087.

70. Murugan R, Kashinath L, Subash R, Sakthivel P, Byrappa K, Rajendran S, Ravi G. Pure and alkaline metal ion (Mg, Ca, Sr, Ba) doped cerium oxide nanostructures for photodegradation of methylene blue. Mater Res Bull. 2018;97:319–25. https://doi.org/10.1016/j.materresbull.2017.09.026.

71. El-Katori EE, Ahmed MA, El-Bindary AA, Oraby AM. Impact of CdS/SnO$_2$ heterostructured nanoparticle as visible light active photocatalyst for the removal methylene blue dye. J Photochem Photobiol A Chem. 2020;392: 112403. https://doi.org/10.1016/j.jphotochem.2020.112403.

72. Miyauchi M, Nakajima A, Watanabe T, Hashimoto K. Photocatalysis and photoinduced hydrophilicity of various metal oxide thin films. Chem Mater. 2002;14(6):2812–6. https://doi.org/10.1021/cm020076p.

73. Ali MH, Al-Afify AD, Goher ME. Preparation and characterization of graphene–TiO$_2$ nanocomposite for enhanced photodegradation of Rhodamine-B dye. Egypt J Aquat Res. 2018;44(4):263–70. https://doi.org/10.1016/j.ejar.2018.11.009.

74. Deniz F, Ersanli E. An efficient biosorbent material for green remediation of contaminated water medium. Int J Phytorem. 2023. https://doi.org/10.1080/15226514.2023.2191742.

Publisher's Note Springer Nature remains neutral with regard to jurisdictional claims in published maps and institutional affiliations.